POLYDISPERSITY EFFECTS FOR DROP CLUSTERS IN A HIGH PRESSURE AND TEMPERATURE ENVIRONMENT[1]

Kenneth G. Harstad* **and Josette Bellan****[2]

Jet Propulsion Laboratory, California Institute of Technology, Pasadena, California, 91109-8099

Abstract

A study of polydisperse clusters of fluid drops at supercritical pressures has been conducted using a previously validated model of subcritical/supercritical isolated fluid drop behavior. Coupled with the isolated drop equations, a set of conservation equations has been developed to describe the global cluster behavior. All these equations are based on the general transport matrix including Soret and Dufour terms and they are consistent with non-equilibrium thermodynamics. Moreover, the model also accounts for real gas effects through accurate equations of state and for correct values of the transport properties in the high pressure, high temperature regime. The model has been exercised for clusters of LO_x drops in H_2 in the range 6-40 MPa. Parametric studies of the effect of the thermal diffusion factor value reveal that the effect of this elusive coefficient is small at 10 MPa and moderate at 40 MPa, and that although the Soret term is dominated by the Fick, Dufour and Fourier terms, it is not negligible. The influence of a cluster Nusselt number is also shown to be relatively small in the range $10^3 - 10^4$ consistent with the supercritical behavior being essentially a diffusive one. All of the results show a nonlinear d^2 variation with curves having a positive curvature independent of the values of the thermal diffusion factor, the Nusselt number or the LO_x/H_2 mass ratio. The approximation of a binary size cluster containing relatively a much larger number of small drops by a monodisperse cluster with a drop size based upon the surface average of the drops in the polydisperse cluster yields a good evaluation of the thermodynamic quantities in the interstitial drop region but an underestimate of the lifetime of the drops in the cluster.

INTRODUCTION

Recent observations of fluid jet breakup at supercritical pressures [1], [2], [3], [4], [5], [6], such as encountered in rocket engine chambers, have identified a fluid disintegration mechanism that is very different from classical atomization. These studies reported a remarkable difference in the outcome of fluid disintegration according to the surrounding pressure: whereas in the subcritical regime ligaments and drops were observed, in the transcritical regime atomization was inhibited, and further in the supercritical regime the subcritically identified ligaments were replaced by thin threads of fluid extruding from the jet in the near field, followed by big chunks of irregularly shaped fluid in the far field. Simple calculations by Candel showed that these big chunks of irregularly shaped fluid are organized in dense clusters. Since previous studies of drop clusters at subcritical pressures have revealed the role of polydispersity for liquid drops [7], the question arises if the same conclusions apply to fluid chunks or drops at supercritical pressures. Because the evaporation of drops at subcritical conditions is a convective-diffusive process, whereas supercritical drop behavior is a diffusive process [9], [10], the inference from one situation to the other may not hold.

The goal of this study is to investigate polydisperse clusters of drops under supercritical conditions by taking as an example a binary size situation. Below we briefly explain a model of supercritical-fluid individual-drop behavior which has been documented in detail elsewhere [8] and further extended to subcritical conditions as well as validated [9], [10] with microgravity data [11] over the entire range of pressures and temperatures of the data. Then, we briefly discuss the drop cluster equations for a polydisperse cluster, noting that a detailed study for a monodisperse cluster has already been performed [12] while the detailed polydisperse equations are presented elsewhere [13]. When analyzing the results, we focus first be understanding the effect of two parameters whose value is relatively uncertain. We also investigate effects of the far field pressure and that of the drop to surrounding fluid mass ratio, and finally explore the merit of the monodisperse approximation.

MODEL

The fluid drop model is based upon Keizer's fluctuation-dissipation theory [14] which has the distinct advantage of formally accounting for non-equilibrium processes as well as naturally relating fluxes and forces for a general fluid, a relationship that continuum theory does not provide. Indeed, it is customary within the continuum formulation to extend the kinetic theory of rari-

[2] *Senior Engineer; **Senior Research Scientist, Associate AIAA Fellow (corresponding author, josette.bellan@jpl.nasa.gov).

fied gases to describe more general cases without a firm justification. The viewpoint of fluctuation theory is intermediate to that of continuum and molecular-level approaches and allows the modeling of transport processes totally consistent with nonequilibrium thermodynamics, which continuum theory does not address. The main result of this theory is the form of the transport matrix which now includes two terms for each the molar and heat fluxes; the molar flux is the sum of Fickian terms and the Soret term, whereas the heat flux term is the sum of the Fourier term and the Dufour term. A detailed description of the model can be found in [8] and [10], and will not be repeated here due to space constraints. This model has been exercised with accurate equations of state [16], accurate transport properties [8], and appropriate boundary conditions [8], [9], [10] without any assumption regarding phase equilibrium. Validation of the single drop model for a binary mixture [9], [10] included the finding of the only unknown transport coefficient, the thermal diffusion factor, from comparison with data. Here the model will be exercised in the context of LO_x/H_2 with values of the thermal diffusion factor inferred from the list in [15].

The configuration is that of a spherical cluster of volume V_C, surface area A_C and radius R_C containing N spherical LO_x fluid drops immersed in quiescent H_2 with far field surroundings denoted by the subscript "e". The N drops are partitioned into K size classes denoted by α and there are N_α drops in each size class with $N = \sum_{\alpha=1}^{\alpha=K} N_\alpha$. We also assume that the interstitial region between drops is uniform and quiescent with respect to the cluster, the implication being that while turbulence is strong enough to mix the interstitial region, it does not affect the regions near the drops. With these definitions, we generalize the monodisperse formulation presented in detail elsewhere [12] to the situation of a polydisperse cluster of fluid drops. As in [12], we define a 'sphere of influence' around each drop that is centered at the drop center and has a radius, R^{si} (superscript "si" refers to sphere of influence), which has a value that is half of the mean distance between adjacent drops, or less. The value of the R^{si} is found from the condition that the spheres of influence must be tightly packed. The Lagrangian value of R^{si} for each size class is R_α and its corresponding volume, V_α, which contains the drop and its surrounding fluid has by definition a fixed mass; this means that the V_α boundary is a function of time to accommodate the change in density due to heating. The volume of the interstitial region of the cluster is $V^i = V_C - \sum_{\alpha=1}^{\alpha=K} N_\alpha V_\alpha$ and it is in this volume that the conservation equations are stated in a Lagrangian frame. These are conservation of mass, species j, and energy, all presented in detail in [13].

One of the distinctive aspects of high pressure behavior is the existence of additional terms in the transport matrix complementing the Fick diffusion in the mass fluxes and the Fourier diffusion in the heat flux; these additional terms are the Soret and Dufour terms, respectively. They state that mass diffusion may occur due to temperature gradients and that heat diffusion may occur due to molar fraction gradients. Associated with these new terms is the new transport coefficient, the thermal diffusion factor. According to the form of the heat flux, one may define two thermal diffusion factors [10], the Irwing-Kirkwood, α_{IK}, and the Bearman-Kirkwood, α_{BK}, which are related through

$$\alpha_{BK} = \alpha_{IK} - \alpha_h, \ \alpha_h \equiv \frac{m_1 m_2}{m^i R_u T^i}\left(\frac{h_1^i}{m_1} - \frac{h_2^i}{m_2}\right), \quad (1)$$

where m_j is the molar mass of species j, $m^i = \sum_{j=1}^{2}(m_j X_j^i)$ where X_j^i is the molar fraction of species j within V^i, h_j^i is the molar enthalpy in V^i, R_u is the universal gas constant and T is the temperature. Following this extended flux matrix model, the heat and mass fluxes at the edge of the sphere of influence for each size class are calculated according to the model of [8]. Similarly, the heat and mass fluxes at the cluster boundary with its surroundings are also calculated according to the formalism introduced in [8].

At the supercritical conditions of the simulations presented below, the fluids no longer obey the perfect gas relationship (instead, they behave according to real gas equations of state), nor the mixture can be considered ideal. Departures from the perfect gas law are quantified by the compression factor, Z

$$Z = \frac{pv}{R_u T}, \quad (2)$$

where p is the pressure and v is the molar volume; for perfect gases $Z = 1$. Similarly, the mixture non-ideality is quantified by the mass diffusion factor, α_D, having a unity value for ideal mixtures. According to the Gibbs-Duhem relationship, for a binary mixture $\alpha_D = \alpha_{D11} = \alpha_{D22} = -\alpha_{D12} = -\alpha_{D21}$, and from thermodynamics

$$\alpha_D = 1 + X_1^i \partial \ln \gamma_1 / \partial X_1^i, \quad (3)$$

where $\gamma_j \equiv \varphi_j/\varphi_j^o$ is the activity coefficient and φ is the fugacity coefficient with the superscript o denoting the pure ($X_j^i = 1$) limit, all within V^i.

At the surface of the spherical cluster we approximate the gradients by a difference across an external length scale r_e

$$\left(\frac{\partial Y_1}{\partial r}\right)_{r=e} = \frac{(Y_{1e} - Y_1^i)}{r_e}, \ \left(\frac{\partial T}{\partial r}\right)_{r=e} = \frac{(T_e - T^i)}{r_e} \quad (4)$$

where Y_1 is the mass fraction of species 1. The length scale r_e may be related to what is equivalent to a Nusselt number, Nu_C, through $r_e = R_C/Nu_C$ since it is the characteristic distance over which transport occurs at the cluster surface. Here, Nu_C is a parameter whose value is prescribed and whose influence will be studied.

The numerical method for obtaining the solution for the variables in each sphere of influence is discussed in detail in [8], [9] and [10]. All simulations were performed on a dual processor 300 MHz personal computer, each run typically lasting 2-3 hours.

RESULTS

Simulations using the above set of equations were performed for an extensive range of parameters but for brevity only those listed in Table 1 will be discussed. All simulations were performed for an extended physical time, up to 0.2 s or 0.25 s, depending on the initial conditions; examination of the results showed that all profiles were already well relaxed by 10^{-2} s, and therefore we will focus the results on the time during which a density gradient is easily identifiable, enabling the optical definition of a drop. This optical definition of the drop does not enter the calculations since the same equations are solved in the entire domain of the sphere of influence including the drop [8], [9],[10]; it is only used for potential comparisons with experiments. The initial drop and far field temperature were 120 K and 1000 K, respectively, and to avoid initial discontinuities, a minute amount of LO_x was assumed to exist in H_2 with a profile that became null in the far field. From the initial LO_x to H_2 mass ratio, ϕ^0, the initial cluster radius, R_C^0, the specified initial drop sizes, $R_{d,\alpha}^0$, and the relative (to N) drop number, the number of drops of each size class was calculated; the present study considers binary sizes of drops. The initial size in the monodisperse cluster of drops was calculated by a surface and drop number averaging, $(R_d^0)^2 = [(R_{d,1}^0)^2 N_1 + (R_{d,2}^0)^2 N_2]/N$, since in such a calculation it is the surface processes that determine fluid interpenetration (be it by diffusion or convection). For all present binary size simulations $R_{d,1}^0 = 4 \times 10^{-3}$ cm, $R_{d,2}^0 = 6 \times 10^{-3}$ cm, and since $N_1/N_2 = 20$; for the monodisperse run, $R_d^0 = 4.12 \times 10^{-3}$ cm. The size class 1 and monodisperse drops having essentially the same initial size, comparisons of the fate of these drops during otherwise similar initial conditions simulations should provide the result of including a small number of large drops in the cluster.

All pressures for which simulations were conducted are above the LO_x critical point (for $LO_x : T_c = 154.6$ K, $p_c = 5.043$ MPa; for $H_2 : T_c = 33.2$ K, $p_c = 1.313$ MPa) so as to simulate a range of conditions pertinent to rocket engine chambers. The equation of state used were those derived in [16] and the viscosity and thermal conductivity were calculated using conventional mixing rules where each species properties were calculated as in [8]. The mass diffusivities calculation over a large range of pressures and temperatures is also described in [8] and the values converge to the liquid and gas ones in the proper limits. A LO_x/H_2 thermal diffusion factor is listed in [15] at one temperature and adopted here as a baseline. To understand the impact of the assumed value of the thermal diffusion factor, a parametric study is conducted below. The value listed [15] being that of α_{BK} (since it is α_{BK} that converges at low pressure to the kinetic theory limit), it is this parameter which will be varied over the listed range.

Effect of the thermal diffusion factor magnitude and of Nu_C

Although for C_7H_{16}/N_2 we determined the approximate values of α_{BK} from comparison with data [9], [10], considering that these values are not usually known, we documented in a previous investigation [19] the effect of α_{BK} and α_{IK} in the context of a C_7H_{16}/N_2 shear layer. We determined that at fixed pressure α_{BK} influences the mixing, being directly related to the molar flux, and α_{IK} influences entrainment through its direct relationship to the heat flux cross term thereby influencing the enthalpy, temperature and density profile. Since these conclusions are dependent on the values of the thermodynamic function α_h, a similar study was conducted for LO_x/H_2 at 20 MPa; additionally, here we also focus on the effect of the value of α_{BK} at different pressures: 10, 20 and 40 MPa. Simulations are performed for $\alpha_{BK} = 0.2$ and 0.5 (Table 1).

Figure 1 plots are of $\alpha_D \nabla Y_1$ and equivalent terms proportional to ∇T in the drop sphere of influence at 5×10^{-3} s, all being calculated from the numerical solution output of the equations, thus explaining the low level fluctuations due to gradients computed on a grid. The results show that in all situations the mass gradient ($\sim \nabla Y$) and thermal gradient ($\sim \nabla T$) terms dominate the Soret term, but that this latter is not negligible and becomes progressively more important with increasing pressure. However, the actual value of α_{BK} affects mainly the Soret term, in agreement with the results from our previous study [19]. Since the Soret term plays only a moderate role in the range of pressures investigated (10-40 MPa), we conclude that lack of knowledge of its exact value will have only a moderate influence on the quantitative (and certainly none on the qualitative) accuracy of the results. The same findings prevail at fixed time for both size classes (Figs. 1a and 1b). For both size classes the mass gradient effect is stronger and the Fourier effect is weaker at larger p_e, this being explained by the faster drop profiles relaxation. Fourier terms reach maximal magnitude closer to the drop boundary than Dufour terms, and the former increase whereas the latter diminish with decreasing α_{BK}; thus the overall variation of the heat flux is not obvious. However, plots of the heat flux (not shown) display a reduced heat flux at the edge of the sphere of influence for smaller α_{BK}, consistent with the higher T^i and smaller ρ^i (not shown), with a consequent increase in R_C and a reduction in the drop number density; the effects are negligible at 10 MPa, but increase with p_e. As for T^i, Y^i and ρ^i at fixed p_e, they are not affected

by α_{BK} since this is a region of uniformity; in fact the magnitude of T^i, Y^i and ρ^i is dominated by the value of Nu_C (not shown).

The influence of Nu_C on a cluster of drops has been documented before [12] and it has been shown that as it increases the cluster expands more rapidly due to increased heat transfer from the far field; however, no conclusions were presented regarding dependence of the d^2 variation upon the value of Nu_C. Figure 1c documents the influence of the Nu magnitude on the present predictions and shows consistently the same increase in fluxes magnitude and the enlargement of the sphere of influence as in [12]. Figure 2a illustrates the optical drop area, A_s, calculated using the location of the maximum density gradient and shows that the d^2- law is not followed as the curves have definite positive curvatures. However, with increasing Nu_C the drops diminish faster, and d^2 has a more linear variation. The departure from the d^2-law has been thoroughly documented elsewhere [10] and has been shown to occur even for pressures closely in excess of the atmospheric. It should be recalled that the d^2- law results from a quasi-steady solution and portrays physics which is different from that of supercritical behavior, and therefore there is no reason to expect it to hold in this regime.

Illustrated in Fig 2b is the corresponding variation of A_s as a function of p_e. Similar to previous results with C_7H_{16}/N_2 [9], [10], even after the initial heat up time during which the drop may sometimes grow in size, the d^2- law is not followed, and this conclusion is independent of the α_{BK} magnitude. However, different from the C_7H_{16}/N_2 behavior, here the d^2- law estimate of the drop lifetime based upon the value of the A_s slope at the end of the heat up period would moderately underestimate the drop lifetime, whereas in our previous study it was shown to considerably overestimate the drop lifetime. It is clear that this aspect is species dependent, and caution should be exercised in inferring conclusions from hydrocarbon-in-N_2 studies to the behavior of LO_x/H_2.

The general conclusions are that ∇Y terms increase and ∇T terms decrease as either p_e or α_{BK} increase, with the ∇T terms being larger for the smaller drops at the smallest p_e. However, all gradient terms increase with Nu_C. The resulting A_s relaxes faster with either increasing p_e or Nu_C, or with decreasing α_{BK}.

Aspects of polydispersity

Smaller versus larger drops behavior

Illustrated in Fig.3 is A_s for 6, 10, 20 and 40 MPa with $\alpha_{BK} = 0.2$; the increase in the drop after the exhibited minimum is an artifact of the calculation as the density has relaxed and the location of the largest gradient is no longer meaningful. Clearly, the optical drop size decreases faster with increasing pressure, however there seems to be a much greater differentiation between the situation at 6 MPa, which is slightly supercritical and the other pressures which are far from the critical point. This finding supports the hydrocarbon/N_2 observations of Nomura et al. [11] and of Sato [20] that the drop lifetime decreases with pressure in the supercritical regime. Moreover, we find that the lifetime of the small drops is considerably smaller, consistent with the quicker temperature (T) rise in the sphere of influence, and consequent higher relaxation rate of the density, ρ, in the same region (not shown); however, the rate of disappearance of the two sizes is similar. It should be realized that the physics of drop disappearance is here quite different from that in the subcritical regime where evaporation and convective-diffusive processes were governing; in contrast, in the supercritical regime the governing phenomenon is only that of diffusion [9], [10], and the emission rate from the drop is null. The 6 MPa local departures from smooth behavior for the larger drops are attributable to the area computation being done at output time stations that are considerably sparser than the time discretization at which the solution is computed and to the enlarged scale of the graph (as a smooth variation appears when plotted over their entire lifetime0.

Monodisperse versus polydisperse clusters

To examine the effect of polydispersity under supercritical conditions we compared 20 MPa results from a monodisperse cluster of drops of 4.12×10^{-3} cm initial radius with those from the two size classes in the binary size cluster. Depicted in Fig. 4 is A_s for these three drop sizes. In a binary size cluster under subcritical conditions the smaller size class would disappear faster than similar size drops in a monodisperse cluster because in the former situation the total mass in the smaller drops is lower with consequent reduced latent heat requirement. Under supercritical conditions we also find that the smaller drops in a binary size cluster with a large N_1/N_2 disappear faster than similar size drops in a monodisperse cluster, although it is no longer due to evaporative processes; instead, due to their smaller size these drops heat up faster inducing a correspondingly faster relaxation of the density. However, the larger size drops persist well after the smaller drops disappear, and therefore when approximating a polydisperse cluster of drops by a monodisperse one, although reproducing well the cluster growth and the interstitial variables values (not shown), one underestimates the cluster lifetime (time when the density gradient is totally relaxed).

Effect of the LO_x/H_2 initial mass ratio

To explore the influence of the LO_x/H_2 initial mass ratio, ϕ^0, we conducted simulations with $\phi^0 = 4, 8$ and 12 (initial values of R^{si} are 1.53×10^{-2} cm, 1.19×10^{-2} cm and 1.03×10^{-2} cm, respectively) at 20 MPa and A_s

is displayed in Fig.5. Consistent with mass diffusional processes in the presence of heat transfer, the drop lifetime is larger with increasing ϕ^0; however, the new result is the increased departure from the d^2-law behavior with increasing ϕ^0. Indeed, when fluid is heated it will expand and reduce gradients as well as fluxes. The extended drop lifetime is attributed to the decreased magnitude of the heat and mass fluxes (not shown). This finding is consistent with that of the Nu_C effect in that with decreasing drop lifetime d^2 assumes a variation close to linear.

Departures from the ideal mixture and perfect gas conditions

Previous studies of the C_7H_{16}/N_2 system [10], [19] have identified considerable departures from the ideal mixture, perfect gas situation. Plots of α_D displayed in Fig. 6a indeed portray mixtures that are non-ideal; all mixtures are initially highly non-ideal tending, as expected, towards ideality as the drops disappear. Radial profiles, such as those in Fig. 6a, always display a minimum at the drop boundary showing that it is there that the mixture is closer to the critical point ($\alpha_D = 0$); values as low as $\alpha_D = 0.2$ are encountered for 6 MPa. Smaller drops have smaller α_D 's, indicating that they may be more prone to reaching critical conditions at the boundary (not shown). Evaluations of Z shown in Fig. 6b illustrate the difference between the state of the drop compared to a liquid: $Z \sim 0.2$ at 6 MPa on the LO_x side of the boundary, indicating that the drop is neither a liquid ($Z \ll 1$) nor an ideal gas ($Z = 1$); however, the state of the drop's surrounding at 6 MPa is essentially that of an ideal gas. With increasing pressure Z increases as well, reaching at 40 MPa values in excess of 1 in both sides of the drop boundary, the value in the initially H_2 side being always larger.

CONCLUSIONS

A model of polydisperse fluid-drop cluster behavior under quiescent far field supercritical thermodynamic conditions has been derived and exercised for LO_x drops in H_2. The formulation is based upon a validated isolated fluid drop model of subcritical and supercritical behavior that included accurate equations of state, and accurate definitions and values of the transport properties. Validation of the isolated drop model required using part of the data for evaluating the thermal diffusion factor for C_7H_{16} drops in N_2. Since a similar data set was not available here, we used as a guideline the low pressure thermal diffusion factor value for N_2 in H_2, and parametrically studied its influence on the results. Comparisons of characteristic gradient terms showed, consistently with other previous results, that the thermal diffusion factor influences mostly the Soret term. This latter, although not negligible, was shown to be dominated both by the mass gradient term (Fick's or Dufour) and by the Fourier term. An increase by a factor of 2.5 in the thermal diffusion factor was shown to yield only modest changes in the Dufour and Soret terms. In fact, the interstitial thermodynamic quantities are insensitive to the value of the thermal diffusion factor up to 40 MPa where a modest sensitivity is apparent. What controls the magnitude of the interstitial quantities is the value of the cluster Nusselt number, however, an order of magnitude increase in the Nusselt number reduces the drop disappearance time only by a small fraction, thus reflecting the diffusive nature (large characteristic times) of the situation.

Under all conditions of this study, encompassing 6-40 MPa and a LO_x/H_2mass ratio of 4-12, the variation of d^2 is not linear and the curves consistently exhibit a positive curvature. Since for the C_7H_{16} drops in N_2 we found consistently a negative curvature, we conclude that this result is species dependent and caution about making hasty inferences from one system of species to another.

Comparisons of results from a binary size cluster of drops containing a much larger proportion of small drops with those from a monodisperse cluster where the drop size is the surface based average of the two size classes shows that although the interstitial quantities may be well predicted by a monodisperse approximation, the lifetime of the cluster is significantly underestimated.

All present results display the departures from the perfect gas law and mixture ideality epitomizing the supercritical conditions. For example, the compression factor exhibits values $O(10^{-1})$ inside the drop which significantly depart from the $O(10^{-3})$ for liquids and $O(1)$ for perfect gases, whereas the mass diffusion factor may decrease as low as 0.2, considerably deviating from the ideal mixture unity value.

ACKNOWLEDGMENT

This research was conducted at the Jet Propulsion Laboratory under sponsorship from the National Aeronautics and Space Administration, the George W. Marshall Space Fight Center with Mr. Klaus W. Gross as technical contract monitor. His continuing interest and support are greatly appreciated.

References

[1] Mayer, W. and Tamura, H., "Flow Visualization of Supercritical Propellant Injection in a Firing LOX/GH2 Rocket Engine", AIAA 95-2433, AIAA/SAE/ASME/ASEE 31st Joint Propulsion Conference, San Diego, CA, 1995

[2] Mayer, W., Schik, A., Schweitzer, C. and Schäffler, M., "Injection and Mixing Processes in High Pressure LOX/GH2 Rocket Combustors", AIAA 96-2620, AIAA/SAE/ASME/ASEE 32nd Joint Propulsion Conference, Lake Buena Vista, FA, 1996

[3] Mayer, W., Ivancic, B., Schik, A. and Hornung, U., "Propellant Atomization in LOX/GH2 Rocket Combustors", AIAA 98-3685, 34th AIAA/ASME/SAE/ASEE Propulsion Conference, Cleveland, OH, 1998

[4] Chehroudi, B., Talley, D. and Coy, E., "Initial Growth Rate and Visual Characteristics of a Round Jet into a Sub- to Supercritical Environment of Relevance to Rocket, Gas Turbine, and Diesel Engines", AIAA 99-0206, 37th Aerospace Sciences Meeting, Reno, NV, 1999

[5] Chehroudi, B., Talley, D. and Coy, E., "Fractal Geometry and Growth Rate Changes of Cryogenic Jets Near the Critical Point", AIAA 99-2489, 35th AIAA/ASME/SAE/ASEE Joint Propulsion Conference, Los Angeles, CA, 1999

[6] Oschwald, M., Schik, A., Klar, M. and Mayer, W., "Investigation of Caoaxial LN2/GH2-Injection at Supercritical pressure by spontaneous Raman Scattering", AIAA 99-2887, 35th AIAA/ASME/SAE/ASEE Joint Propulsion Conference, Los Angeles, CA, 1999

[7] Harstad, K. and Bellan, J., "Behavior of a Polydisperse Cluster of Interacting Drops in an Inviscid Vortex", *Int. J. of Multiphase Flow*, 23(5), 899-925, 1997

[8] Harstad, K. and Bellan, J., "Isolated Fluid Oxygen Drop Behavior in Fluid Hydrogen at Rocket Chamber Pressures", *Int. J. Heat Mass Transfer*, 41, 3537-3550, 1998

[9] Harstad, K. and Bellan, J., "A Validated All-Pressure Fluid Drop Model for Binary Mixtures: Heptane in Nitrogen", paper AIAA 99-206, Joint AIAA/ASME/SAE Propulsion Meeting, Los Angeles, CA, June 20-23, 1999

[10] Harstad, K. and Bellan, J., "An All-Pressure Fluid Drop Model Applied to a Binary Mixture: Heptane in Nitrogen", accepted for publication in the *Int. J. of Multiphase Flow*, 1999

[11] Nomura, H., Ujiie, Y., Rath, H. J., Sato, J. and Kono, M., "Experimental Study on High Pressure Droplet Evaporation Using Microgravity Conditions", *26th Symp. (Int.) on Comb.*, 1267-1273, 1996

[12] Harstad, K. and Bellan, J., "Interactions of Fluid Oxygen Drops in Fluid Hydrogen at Rocket Chamber Pressures", *Int. J. Heat Mass Transfer*, 41, 3551-3558, 1998

[13] Harstad, K. and Bellan, J., "The d^2 variation for polydisperse clusters of LOX drops in Hydrogen at supercritical conditions", submitted to the Proc. Int. Symp. Comb., Vol. 28, 2000

[14] Keizer, J. 1987 Statistical thermodynamics of nonequilibrium processes, Springler-Verlag, New York

[15] Chapman, S. and Cowling, T. G., The Mathematical Theory of Nonuniform Gases Cambridge University Press, Cambridge, 1970

[16] Harstad, K., Miller, R. S. and Bellan, J., "Efficient High-Pressure State Equations", *A.I.Ch. E. J.*, 43(6), 1605-1610, 1997

[17] Sarman, S. and Evans, D. J., "Heat flux and mass diffusion in binary Lennard-Jones mixtures", *Phys. Rev.*, A45(4), 2370-2379, 1992

[18] Reid, R. C., Prausnitz, J. M. and Polling, B. E., The Properties of Gases and Liquids, 4th Edition, McGraw-Hill Book Company, 1987.

[19] Miller, R. S., Harstad, K. G. and Bellan, J., "Direct Numerical Simulations of Supercritical Fluid Mixing Layers Applied to Heptane-Nitrogen", submitted to *J. Fluid Mech.*, 1999

[20] Sato, J., "Studies on droplet evaporation and combustion in high pressures", AIAA 93-0813 31^{st} Aerospace Sciences Meeting Jan. 11-14, Reno, NV, 1993

Run	p, MPa	α_{BK}	ϕ^0	Nu_C
d6a	6	0.2	8	10^3
d10a	10	0.2	8	10^3
d20a	20	0.2	8	10^3
d40a	40	0.2	8	10^3
d10b	10	0.5	8	10^3
d20b	20	0.5	8	10^3
d40b	40	0.5	8	10^3
d20c	20	0.5	4	10^3
d20d	20	0.5	12	10^3
d20e	20	0.2	8	10^4
s20	20	0.5	8	10^3

Table 1: List of simulations discussed. Names starting with "d" are for binary size clusters and those starting with "s" for single size. The drop's initial temperature was 120 K and the far field temperature was 1000 K in all simulations. The cluster radius was 1.25 cm in all calculations.

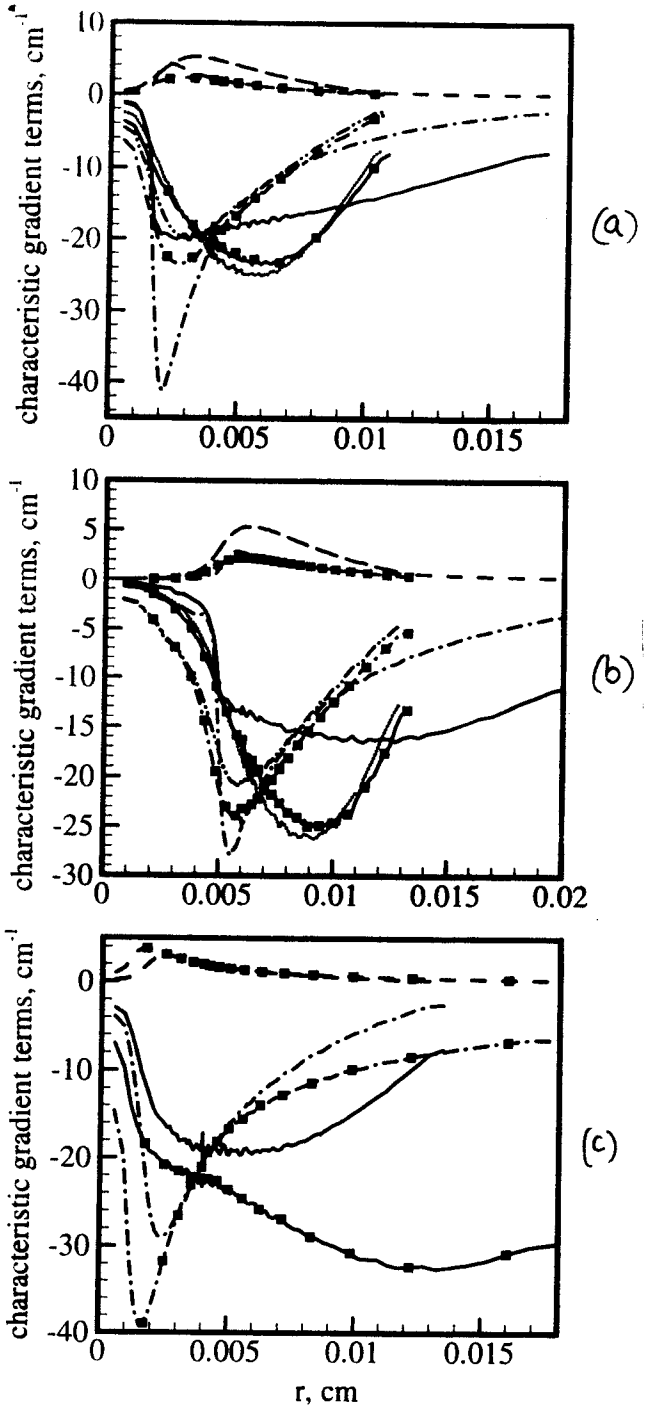

Figure 1. Characteristic gradient terms for the mass, Soret and Fourier contributions (the mass term is the Dufour term in the heat flux) at $t = 5 \times 10^{-3}$ s. (1a): influence of α_{BK} as function of p for $R_{d,1}$. (1b) influence of α_{BK} as function of p for $R_{d,2}$.(1c): influence of Nu at $p = 20$ MPa for $R_{d,1}$. For 1a and 1b: mass gradient terms 10 MPa, $\alpha_{BK} = 0.2$ (——); 40 MPa, $\alpha_{BK} = 0.2$ (—■—); 40 MPa, $\alpha_{BK} = 0.5$ (· · ·); Soret terms 10 MPa, $\alpha_{BK} = 0.2$ (- - - -); 40 MPa, $\alpha_{BK} = 0.2$ (- -■ - -); 40 MPa, $\alpha_{BK} = 0.5$ (— —); Fourier terms 10 MPa, $\alpha_{BK} = 0.2$ (— · — · —); 40 MPa, $\alpha_{BK} = 0.2$ (— · ■ — · —); 40 MPa, $\alpha_{BK} = 0.5$ (— · — · — · —). (1c) 20 MPa results: mass gradient terms $Nu = 10^3$ (——), $Nu = 10^4$ (—■—); Soret terms $Nu = 10^3$ (- - - -), $Nu = 10^4$ (- -■ - -); Fourier terms $Nu = 10^3$ (— · — · —), $Nu = 10^4$ (— · ■ — · —).

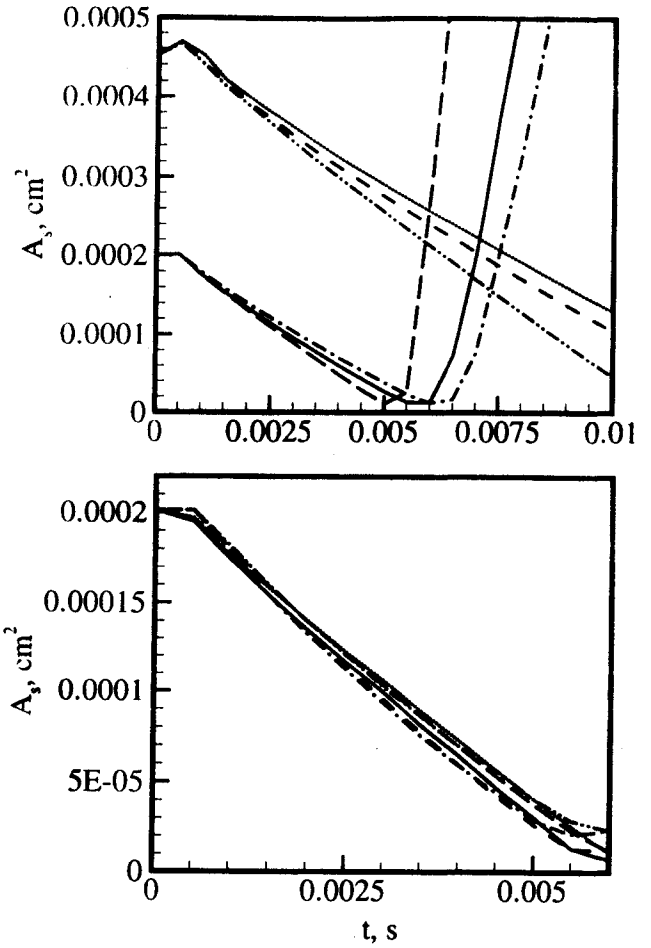

Figure 2. Time variation of the drop area corresponding to Runs d20a [$R_{d,1}$ (——); $R_{d,2}$ (- - - -)]; d20b [$R_{d,1}$ (— · — · —); $R_{d,2}$ (· · ·)]; d20e [$R_{d,1}$ (— —); $R_{d,2}$ (— · — · — · —)] in 2a; and Runs d10a (——); d20a (- - - -); d40a (— · — · —); d10b (· · ·); d20b (— —); d40b (— · · — · · —) for $R_{d,1}$ in 2b.

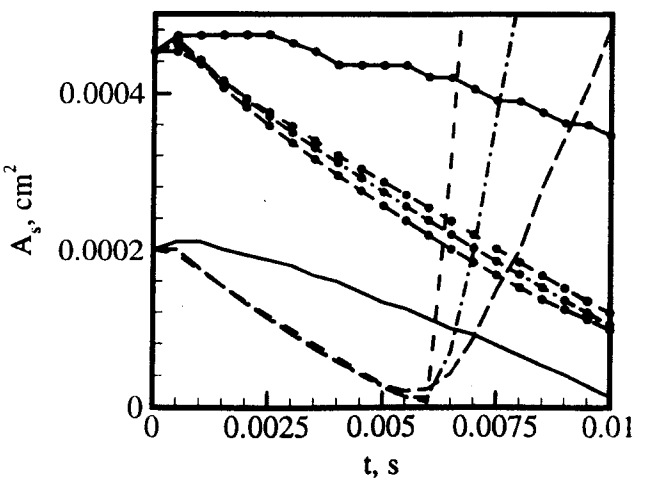

Figure 3. Time variation of the drop area corresponding to Runs d6a [$R_{d,1}$ (——); $R_{d,2}$ (—•—)]; d10a [$R_{d,1}$ (- - - -); $R_{d,2}$ (- - •- -)]; d20a [$R_{d,1}$ (— · — · —); $R_{d,2}$ (— · • — · —)]; d40a [$R_{d,1}$ (— —); $R_{d,2}$ (— •—)].

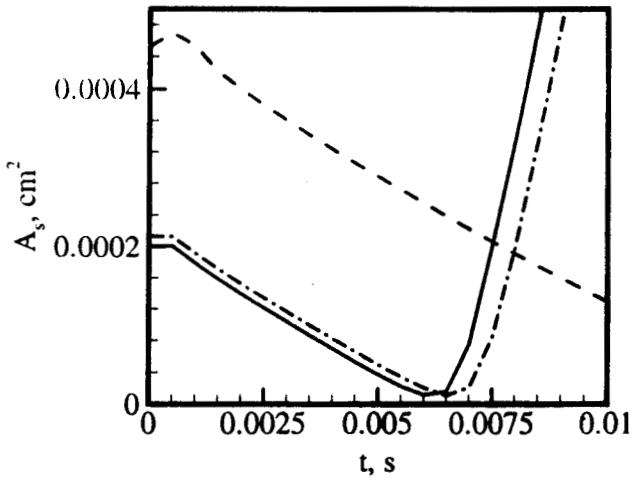

Figure 4. Time variation of the drop area corresponding to Runs d20b [$R_{d,1}$ (——); $R_{d,2}$ (- - - -)] and s20 (— · — · —).

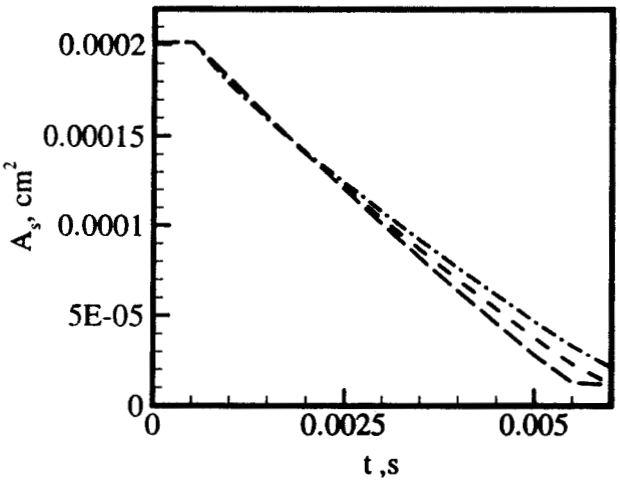

Figure 5. Time variation of the drop area corresponding to $R_{d,1}$ in Runs d20c (— —); d20b (- - - -); and d20d (— · — · —).

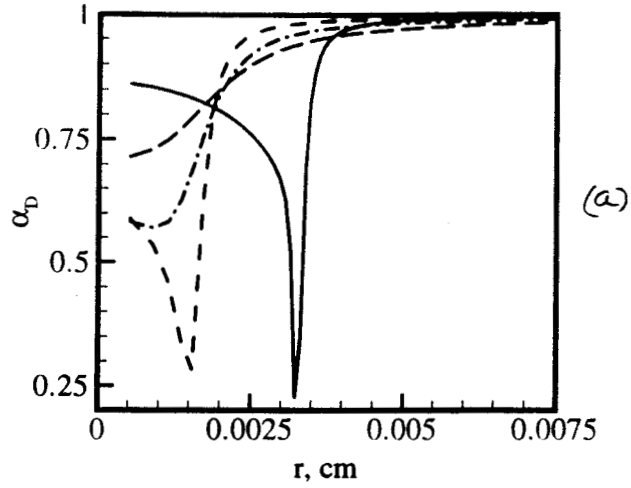

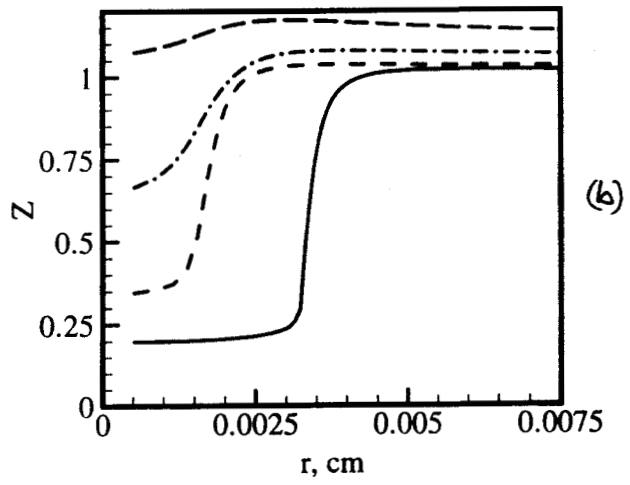

Figure 6. Radial variation of the mass diffusion factor (6a) and compression factor (6b) in the drop sphere of influence for size class 1 for 6 MPa (——), 10 MPa (- - - -), 20 MPa (— · — · —) and 40 MPa (— —) corresponding to Runs d6a - d40a.